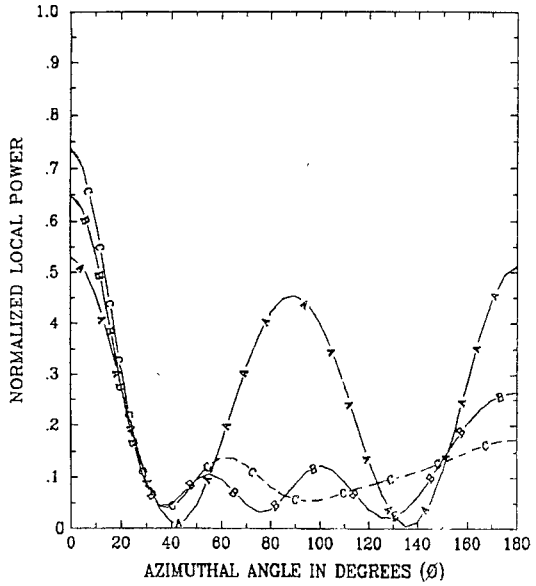

Fig. 3 Local power dissipation for the array focused at $\rho = \rho_f = 0.5a$ as a function of the azimuthal coordinate for $\rho = 0.5$ a, where the A, B, and C curves correspond to $N = 4$, 8, 16, respectively (Note that curve C does not show the details of the ripples, see text.)

Using the values of δ_n indicated above, the normalized local power P is shown plotted in Fig. 2 as a function of the normalized radial distance ρ/a for $\phi = 0^0$ for the three cases $N = 4$, 8, 16. As indicated, there is a significant enhancement of the power dissipation in the region of the focus point $\rho_f/a = 0.5$. Furthermore, the focus is most pronounced for the case of $N = 16$. To give some idea of the azimuthal variation of the power levels, P is plotted in Fig. 3 for the same condition, as a function of the angle ϕ, and for fixed $\rho/a = 0.5$. Here, we see rather dramatically that there are noticeable secondary "hot spots" for the $N = 4$ case at the 90^0 points. On the other hand, for the $N = 8$ and $N = 16$ cases, the secondary maxima do not appear. Not surprisingly, we see that the ripples in the azimuthal variation become greater in number as N increases. (Actually this detail is not evident in Fig. 3 for the $N = 16$ case because of computational limitations.)

IV. Concluding Remarks

The limitations for controlling the local power dissipation in a cylindrical target are rather severe. We have attempted to illustrate the problem with a two-dimensional model consisting of a concentric aperture array system with a prescribed form of excitation. It is confirmed that some power enhancement takes place at the focus point, but care must be taken to account for secondary foci where additional "hot spots" may occur. The latter will occur when the number of aperture elements in the array are insufficient and/or the electrical size of the cylinder is large, such that significant phase interference occurs between the individual aperture contributions at other than the desired focus point. Further investigations that deal with the aperture design problem are underway. One possible scheme is to modify the relative amplitude factors Δ_n of the individual apertures to reduce the spurious "hot spots," but care must be taken not to accomplish this at the expense of greater heating of the peripheral regions of the target. It would also be useful to extend the present numerical scheme to three-dimensional models (i.e., the axially-bounded aperture for layered cylindrical models) such as treated by Ho, Guy, Sigelmann, and Lehman [3]. These investigators, however, did not explicitly consider focusing.

Acknowledgment

The authors would like to thank Dr. T. Cetas of the University Health Sciences Center for his help and encouragement. The comments from Dr. D. G. Dudley are also appreciated.

References

[1] J. R. Wait, "Focused heating in cylindrical targets," *IEEE Trans Microwave Theory Tech.*, vol. MTT-32, pp. 647–649, July 1985
[2] C C Johnson and A. W Guy, "Properties of electromagnetic waves in muscle tissue," *Proc IEEE*, vol 60, pp 692–700, Apr. 1972
[3] H S Ho, A W Guy, R A. Sigelmann, and J. F. Lehmann, "Microwave heating of simulated limbs by aperture sources," *IEEE Trans. Microwave Theory Tech.*, vol. MTT-19, pp. 224–231, Feb. 1971

Numerical Analysis of Various Configurations of Slab Lines

GIOVANNI B. STRACCA, GIUSEPPE MACCHIARELLA, AND MARCO POLITI

***Abstract*—Numerical solutions are presented for the characteristic impedance of various line structures derived from the slab line, which allow the calculation also of the even and odd impedance of coupled slab lines. Some approximated formulas are also derived, which match the numerical results with good precision for a large range of geometrical dimensions of the structures.**

The results presented here are compared with some formulas and numerical results available from previous technical papers.

I. Introduction

In this paper, both numerical solutions and analytical interpolating formulas are presented for the characteristic impedance of the various transmission-line structures shown in Fig. 1. The structure in Fig. 1(a) is the well-known slab line, which is composed of a cylindrical metallic rod of diameter d, placed symmetrically between two parallel ground planes AA' and BB' at a distance h. The structure of Fig. 1(b), known as the trough line, and that of Fig. 1(c) are derived from the slab line by introducing in Section CD an electric conductor plane (short circuit) (Fig. 1(b)) or a magnetic conductor plane (open circuit) (Fig. 1(c)), orthogonal to the ground planes and at a distance $c/2$ from the center of the rod.

The characteristic impedance of the structure of Fig. 1(b) is equal to the odd characteristic impedance Z_{co} of two-coupled equal slab lines (Fig. 2), separated by a distance c; in addition, the characteristic impedance of the structure in Fig. 1(c) is also equal to the even characteristic impedance Z_{ce} of the structure in Fig. 2. Both characteristic impedances of the two transmission lines of Fig. 1(b) and (c) approach the characteristic impedance Z_c of the slab line, when the distance $c/2$ is very large.

Manuscript received June 25, 1985; revised October 29, 1985
G. B Stracca and M. Politi are with the Dipartimento di Elettronica, Politecnico di Milano, Piazza Leonardo da Vinci 32, 20133 Milano, Italy.
G Macchiarella is with Centro di Studio Per le Telecomunicazioni Spaziali del CNR, Via Ponzio 34/5, 20133 Milano, Italy.
IEEE Log Number 8406852.

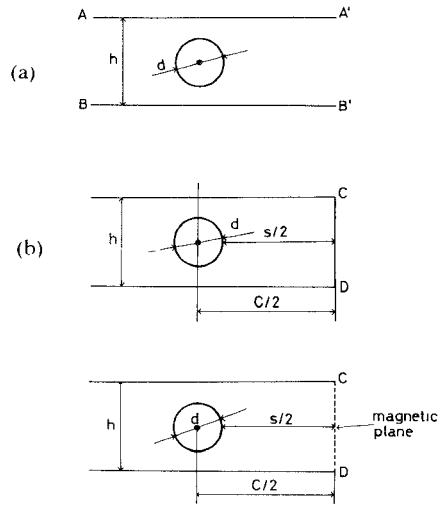

Fig. 1. Various transmission lines derived from the slab line.

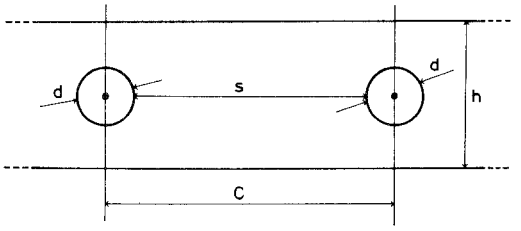

Fig. 2. Coupled slab lines.

The characteristic impedances of the various slab lines of Fig. 1 have been obtained by numerically evaluating the static capacitance per unit length of these structures: the moments method with a point-matching technique has been employed for the solution of the problem. Interpolating expressions have been further obtained, which give the characteristic impedances with a good approximation, as functions of the geometrical dimensions of the transmission lines. From the results presented here, either in their numerical form or, more easily, by means of the analytical formulas, it is possible to perform calculations for all the structures composed by slab lines (for example, directional couplers, and comb and interdigital filters [1]).

Finally, some comparisons are discussed between the results presented in the paper and the data available in the literature; in particular, the works of Chilshom [2] and Cristal [3] have been considered (the computed data required to be suitably transformed, as explained in Section V, in order to refer to the slab-line structures of Fig. 3).

II. Evaluation of the Characteristic Impedances of the Slab-Line Structures

The evaluation of the characteristic impedance of a TEM mode in a lossless uniform transmission line can be reduced to that of a dc capacitance per unit length C between the two conductors of the line.

In fact, Z_c depends on C through the relationship

$$Z_c = \frac{Z_\infty}{\sqrt{\epsilon_r}} \frac{\epsilon}{C} \tag{1}$$

where ϵ_r is the relative permittivity of the propagation medium, and $Z_\infty = \sqrt{\mu_0/\epsilon_0} = 376.73\ \Omega$ is the free-space wave impedance.

The static capacitance per unit length C of a transmission line is equal to the total electric charge per unit length Q on one of

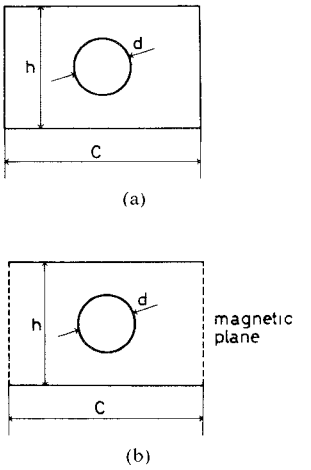

Fig. 3. Slab-line structures considered in [3]

the two conductors, when a potential difference $V=1$ is applied between the two conductors. To perform this computation numerically, the inner cylindrical conductor has been replaced with a finite number N of line charges q_j (with $j=1$ to N) placed on a circle of radius $r < d/2$, inside the inner cylindrical conductor; the values of the charges q_j—the sum of which $Q=\Sigma_j q_j$ represents the solution of the problem—can then be obtained by imposing a constant potential at several points on the surface of radius $d/2$, corresponding to the surface of the inner conductor; in particular, if the number of points is the same as the line charges, a point-matching solution of the problem can be obtained, with a precision depending on the number N of line charges q_j considered.

To take into account the boundary conditions imposed by electric or magnetic planes in the two structures of Fig. 1(b) and (c), the images method has been used, replacing the electric and magnetic planes with an infinite set of image charges. The structure of Fig. 1(a) can be seen as a particular case of Fig. 1(b) and (c) structures, when the distance $c/2$ becomes very large.

Two kinds of errors are unavoidably introduced evaluating Z_c, Z_{c0}, and Z_{ce} numerically, according to the present method. The first one arises from the finite number of images that can be taken into account; the second one is due to the finite number N of discrete line charges that approximate the actual continuous charge distribution on the surface of the inner conductor. As a consequence of the finite number N, the potential V is constant only at the N points and not on the whole surface.

The first kind of error becomes in practice very small if only a few tens of images are considered; however, this summation continues in the computer program as long as the relative contribution of the following term becomes less than 10^{-4}.

In order to reduce the second kind of error, the number N of line charges on the circle of radius r was chosen large enough (e.g., typically 32). Moreover, for each d/h ratio, the value of r/d, which gives the minimum deviation ΔV from $V=1$ of the potential in the middle of two observation points on the surface of the cylindrical rod, was employed. This deviation ΔV was found to be better than $5\ 10^{-6}$ for $d/h \leqslant 0.9$ and $N=32$; ΔV remains better than $3.7\ 10^{-4}$ up to $d/h=0.99$ when $N=64$. The value of the optimum r/d decreases from 0.375 when $d/h=0.1$ to 0.28 when $d/h=0.9$, with $N=32$. It increases to 0.42 when $d/h=0.99$ if $N=64$. However, it must be noticed that the influence of both r/d and N (the number of line charges) on the computed values of Z_c is not very critical when N is sufficiently large (at least 16). For instance, the variation

TABLE I
COMPUTED VALUES OF THE ODD CHARACTERISTIC IMPEDANCE
(Fig. 1(b))

d/h =	0.10	0.20	0.30	0.35	0.40	0.50	0.60	0.70	0.80	0.90
c/2h										
0.10	77.50	-	-	-	-	-	-	-	-	-
0.15	101.89	55.23	-	-	-	-	-	-	-	-
0.20	116.86	73.26	44.12	29.66	-	-	-	-	-	-
0.25	126.96	84.46	58.20	47.31	36.79	-	-	-	-	-
0.30	134.05	92.03	66.81	56.88	47.94	31.18	-	-	-	-
0.35	139.12	97.31	72.57	63.01	54.59	39.95	26.44	-	-	-
0.40	142.77	101.09	76.55	67.16	58.95	45.02	33.17	22.06	-	-
0.50	147.35	105.76	81.37	72.08	64.01	50.45	39.24	29.56	20.83	12.42
0.60	149.77	108.21	83.86	74.58	66.53	53.02	41.84	32.17	23.40	14.78
0.70	151.08	109.51	85.17	75.89	67.83	54.30	43.09	33.34	24.41	15.46
0.80	151.76	110.19	85.85	76.58	68.52	54.98	43.72	33.90	24.66	15.72
0.90	152.12	110.56	86.22	76.94	68.88	55.32	44.05	34.20	25.10	15.90
1.00	152.32	110.74	86.41	77.13	69.08	55.50	44.22	34.35	25.22	15.95
1.50	152.53	110.97	86.62	77.34	69.29	55.70	44.41	34.51	25.34	16.03
2.00	152.53	110.98	86.63	77.35	69.30	55.72	44.42	34.52	25.34	16.03
∞	152.54	110.98	86.63	77.35	69.30	55.72	44.42	34.52	25.34	16.03

TABLE II
COMPUTED VALUES OF THE EVEN CHARACTERISTIC IMPEDANCE
(Fig. 1(c))

d/h =	0.10	0.20	0.30	0.35	0.40	0.50	0.60	0.70	0.80	0.90
c/2h										
0.10	220.68	-	-	-	-	-	-	-	-	-
0.15	200.63	155.34	-	-	-	-	-	-	-	-
0.20	187.06	143.73	116.39	105.25	-	-	-	-	-	-
0.25	177.56	135.08	109.10	98.71	89.37	-	-	-	-	-
0.30	170.76	128.69	103.46	93.53	84.68	69.13	-	-	-	-
0.35	165.83	124.01	99.16	89.49	80.96	66.10	53.12	-	-	-
0.40	162.25	120.53	95.91	86.39	78.04	63.66	51.21	39.83	-	-
0.50	157.72	116.11	91.67	82.30	74.13	60.22	48.41	37.76	27.61	17.19
0.60	155.31	113.73	89.34	80.03	71.92	58.21	46.66	36.39	26.71	16.74
0.70	154.03	112.44	88.10	78.79	70.71	57.07	45.65	35.57	26.12	16.46
0.80	153.34	111.76	87.42	78.13	70.05	56.44	45.09	35.09	25.78	16.28
0.90	152.96	111.41	87.05	77.77	69.70	56.11	44.78	34.83	25.59	16.16
1.00	152.78	111.20	86.85	77.57	69.51	55.92	44.61	34.69	25.48	16.11
1.50	152.57	110.99	86.64	77.36	69.30	55.72	44.43	34.53	25.36	16.04
2.00	152.54	110.99	86.63	77.35	69.29	55.72	44.42	34.52	25.35	16.02
∞	152.54	110.98	86.63	77.35	69.30	55.72	44.42	34.52	25.34	16.03

obtained in Z_c varying N from 32 to 64 was above a few percent only for $d/h = 0.99$, although the ΔV error with $N = 32$ was in this case not very small ($\Delta V = 1.43\ 10^{-2}$).

III. Results of the Numerical Computations

The results of the computations of Z_c (Fig. 1(a)), Z_{co} (Fig. 1(b)) and of Z_{ce} (Fig. 1(c)) are presented in Table I (Z_{co}) and in Table II (Z_{ce}) for several values of d/h and c/h. The value of Z_c is given as that of Z_{co} and Z_{ce} in case of $c/h = \infty$. For three value of d/h (0.1,0.5,0.9), the computed values of Z_{ce} and Z_{co} are also reported in graphical form in Fig. 4.

IV. Analytical Approximations for Z_C, Z_{CO}, Z_{CE}

It is possible to derive, from the numerical results, analytical interpolating formulas for Z_c, Z_{co}, and Z_{co}, and Z_{ce}.

The formulas presented here have been derived by slightly modifying the following well-known approximated expression of the characteristic impedance of the slab line [4]:

$$Z_c = \frac{Z_\infty}{2\pi} \ln\left(\frac{4}{\pi d/h}\right) \tag{2}$$

where Z_∞ is the wave impedance of the propagation medium. Equation (2) is a good approximation for small values of d/h (< 0.3). A correcting coefficient F, which depends on d/h, has been introduced in this equation for a better match with the numerical values of Z_c, obtained for greater values of d/h

$$Z_c = \frac{Z_\infty}{2\pi} \ln\left(\frac{4}{\pi \frac{d}{h} F}\right). \tag{3}$$

The following expression for F has proved to be satisfactory up to $d/h \leqslant 0.95$

$$F = \left[1 - \left(\frac{d}{h}\right)^4 \Big/ 5.905\right]^{1/2} \left[1 + \exp\left[16\left(\frac{d}{h} - 1.142\right)\right]\right]. \tag{4}$$

The precision of the interpolating formulas (3) and (4) is better than 0.01 percent for $d/h \leqslant 0.9$, assuming as reference the computed values of Z_c, and grows to 2.2 percent for $d/h = 0.95$.

Expressions similar to (3) also can be employed for the characteristic impedance of the structures in Fig. 1(b) and (c) introducing two additional correcting coefficients F_e and F_o

$$Z_{co} = \frac{Z_\infty}{2\pi} \ln\left[4 \Big/ \left(\pi \frac{d}{h} F F_o\right)\right] \tag{5}$$

$$Z_{ce} = \frac{Z_\infty}{2\pi} \ln\left[4 \Big/ \left(\pi \frac{d}{h} F F_e\right)\right] \tag{6}$$

where F is given again by (4). The new coefficients F_e and F_o,

which depend in general both on c/h and d/h, can be given by the following expressions, obtained from the approximated formulas for Z_{ce} and Z_{co} reported in [5], [6] by introducing the correcting coefficients M_e and M_o:

$$F_o = M_o \coth(\pi c/2h) \tag{7}$$

$$F_e = M_e \tanh(\pi c/2h). \tag{8}$$

The factors M_e and M_o are very close to 1 and can be evaluated from the computed values of Z_{ce} and Z_{co}; therefore, suitable interpolating expressions have been found, which give the min–max error between the computed impedances and those obtained from the formulas (5)–(8)

$$M_e = 1 + \exp\left[\left(a_1x^2 + a_2x + a_3\right)y\right] - \exp\left[\left(a_4x^2 + a_5x + a_6\right)y\right] \tag{9}$$

$$M_o = 1 + \exp\left[\left(b_1x^2 + b_2x + b_3\right)y\right] - \exp\left[\left(b_4x^2 + b_5x + b_6\right)y\right] \tag{10}$$

where $x = d/h$ and $y = (c-d)/d = s/d$; the coefficients a_i and b_i are given by

$$\begin{aligned} a_1 &= -1.8861 & b_1 &= 3.0989 \\ a_2 &= 1.4177 & b_2 &= -8.2997 \\ a_3 &= -5.5142 & b_3 &= -3.0843 \\ a_4 &= -2.7030 & b_4 &= 4.0797 \\ a_5 &= 4.6772 & b_5 &= -2.1808 \\ a_6 &= -8.5900 & b_6 &= -8.5534 \end{aligned}$$

The maximum percent error between the computed and the interpolated values of the impedances is 1.4 percent for Z_{ce} and 3.2 percent for Z_{co}, for $d/h \leqslant 0.9$ and for $s/d \geqslant 0.3$. In Fig. 4, both interpolated and computed values of Z_{ce} and Z_{co} are reported as functions of s/h, for some values of d/h. It can be seen from the figure that the largest deviations between computed and interpolated impedances occur for large values of $d/h (d/h > 0.5)$.

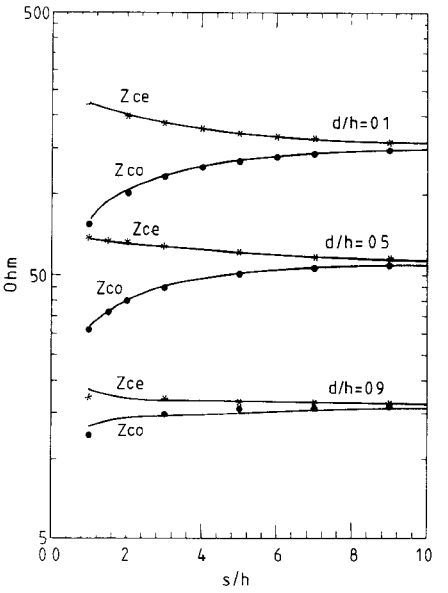

Fig 4 Computed (stars and points) and interpolated (continuous lines) values for the even and odd impedances of coupled slab lines

V. Comparison Between Numerical Calculations and Available Results

A. Comparison with the Results Given in [2]

In [2], Chisholm has employed a variational method to compute the characteristic impedances of the structures in Fig. 1(a) and (b); however, only three values of c/h were considered in [2]. The comparison with the impedance values here computed for $c/h = 0.5$, 1, and 1.5 shows that the difference is smaller than 1 percent for $d/h < 0.6$, but grows to 2.5 percent for Z_c and to 6.5 percent for Z_{co} for $d/h = 0.9$, i.e., for the larger values of d/h, where the procedure employed in [2] is no longer satisfactory. In addition, no results were given in [2] for the structure of Fig. 1(c) (i.e., for Z_{ce}).

B. Transformation of the Formulas Given in [3]

The formulas obtained by Cristal in [3] refer to the structures of Fig. 3(a) and (b) and cannot be used directly for the structures of Fig. 1. However, it is possible to arrange a suitable transformation in order to apply these formulas to the structures in Fig. 1(b) and (c).

In fact, for the structures of Fig. 3(a) and (b), it is possible to divide the total capacitance per unit length C_o of Fig. 1(b) structure into two parts C_e and C_s, where C_e is the capacitance considered in Fig. 1(c) and C_s the capacitance towards the short-circuit plane CD. Furthermore, C_e may be divided into two parts: C_g and C_∞. C_g is the capacitance considered in Fig. 3(b) and C_∞ the residual capacitance.

It is possible, therefore, to write the total capacitance of the structure in Fig. 3(a) as $C_g + 2C_s$ and that of the structure in Fig. 1(c) as $C_g + C_\infty$. The relationship between the characteristic admittances Y_c, Y_{co}, and Y_{ce} of the three structures shown in Fig. 1 and the characteristic admittances Y'_{ce} and Y'_{co} of the two structures shown in Figs. 3(a) and (b) is given by the following:

$$Y_{ce} = (1/2)(Y_c + Y'_{ce}) \tag{11}$$

$$Y_{co} = (1/2)(Y_c + Y'_{co}). \tag{12}$$

The admittances Y'_{ce} and Y'_{co} can be obtained either from the capacitances C_g and C_s, computed numerically in [3], or from the approximated analytical expressions obtained by replacing the rod with an infinitesimal line charge located at the axis of the rod [3]

$$Z'_{co} = \frac{Z_\infty}{2\pi\sqrt{\epsilon_r}} \left[\ln\left\{ \frac{(d\pi/4h)}{\sqrt{\left|1-\left(\frac{d}{2h}\right)^4\right|\left|1-\left(\frac{d}{2c}\right)^4\right|}} \right\} + 2\sum_1^\infty (-1)^m \ln\left\{ \tanh\left(m\frac{\pi}{2}\frac{c}{h} \right) \right\} \right] \tag{13}$$

$$Z'_{ce} = \frac{Z_\infty}{2\pi\sqrt{\epsilon_r}} \left[\ln\left\{ \frac{(d\pi/4h)\left|1-(d/2c)^4\right|^{1/2}}{\sqrt{1-\left(\frac{d}{2h}\right)^4}} \right\} + 2\sum_1^\infty \ln\left\{ \tanh\left(m\frac{\pi}{2}\frac{c}{h} \right) \right\} \right]. \tag{14}$$

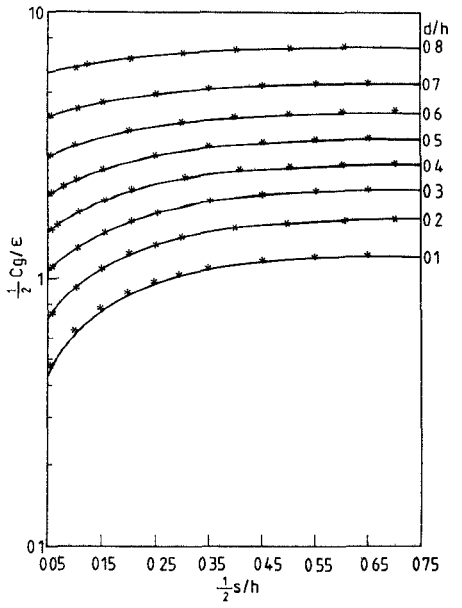

Fig. 5. Comparison between $C_g/(2\epsilon)$ as computed in [3] (continuous line) and the computed values here obtained (stars).

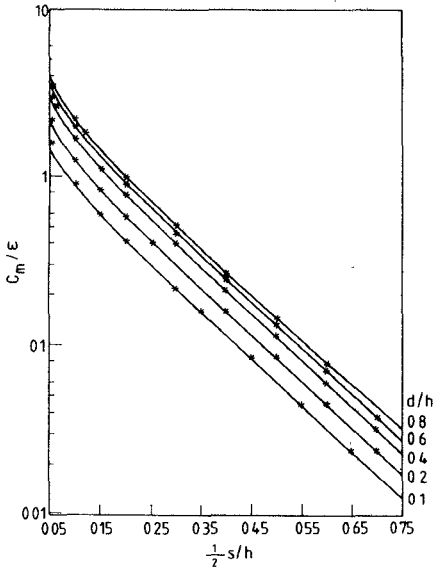

Fig. 6. Comparison between C_m/ϵ as computed in [3] (continuous line) and the computed values here obtained (stars).

Notice that the above expressions give a satisfactory approximation of the actual admittances (maximum percent error less than 1 percent [3]) only for $d/h < 0.3$ and $s/d > 2$, which are quite below the limits on d/h and s/d considered in the interpolating formulas given in this paper.

C. Comparison with the Numerical Results Given in [3]

Figs 2 and 3 in [3] show the numerical results obtained by Cristal for the structures in Fig. 3(a) and (b), as static capacitances C_g/ϵ and C_m/ϵ, where $C_m = 1/2C_s$.

For the purpose of comparison, the numerical results obtained here have been transformed into the same form given by Cristal. With the same procedure adopted in Section V-B, we obtain from (11) and (12)

$$Y'_{co} = 2Y_{co} - Y_c \tag{15}$$

$$Y'_{ce} = 2Y_{ce} - Y_c. \tag{16}$$

As a consequence, the Cristal's parameters C_g/ϵ and C_m/ϵ may be written as a function of Y_{co}, Y_{ce}, and Y_c

$$C_g/\epsilon = Z_\infty(2Y_{ce} - Y_c) \tag{17}$$

$$C_m/\epsilon = Z_\infty(Y_{co} - Y_{ce})/2. \tag{18}$$

The graphs of [3] for $\frac{1}{2}C_g/\epsilon$ and C_m/ϵ are shown in Figs. 5 and 6 together with some points representing the numerical results obtained in this work, transformed for the structure of Fig. 3 by means of (17) and (18). The figures show a very good agreement between the results obtained with the numerical method followed in this paper and those given by Cristal.

VI. Conclusion

A numerical evaluation of the characteristic impedance of slab line and of two derived transmission lines has been presented. The results obtained in the case of these two structures also represent the even and odd characteristic impedance of two coupled slab lines.

The results obtained show a very good agreement when compared with the few available data in the literature. An extensive comparison of the computed values has been made, in particular with the data presented by Chisholm [2] and Cristal [3]. In addition, the overall accuracy of the numerical method employed has been estimated and seems better than 1 percent for the computed values of the characteristic impedance of all the transmission lines considered, when $d/h \leqslant 0.9$ and $s/d \geqslant 0.1$.

Closed-form expressions for the characteristic impedances considered here have also been presented, and were obtained by interpolating the numerical values. The precision of these expressions, if compared with the numerical values, is better than 1 percent for the characteristic impedance of the slab line and about 1.5 and 3 percent for even and odd characteristic impedance of coupled slab lines, respectively.

References

[1] G. B. Stracca, G. Macchiarella, G. Dolci, and M. Politi, "Design formulas for coupled slab lines," *Alta Frequenza*, vol. 54, pp. 346–352, Dec. 1985.
[2] R. M. Chisholm, "The characteristic impedance of trough and slab lines," *IRE Trans. Microwave Theory Tech.*, vol. MTT-4, pp. 166–177, July 1956.
[3] E. G. Cristal, "Coupled circular cylindrical rods between parallel ground planes," *IRE Trans. Microwave Theory Tech.*, vol. MTT-12, pp. 428–439, July 1964.
[4] S. Frankel, "Characteristic impedance of parallel wires in rectangular troughs," *Proc. IRE*, vol. 30, pp. 182–190, Apr. 1942.
[5] J. T. Bolljahn and G. L Matthaei, "A study of the phase and filter properties of arrays of parallel conductors between ground planes," *Proc. IRE*, vol. 50, pp. 299–311, Mar. 1962.
[6] R. Levy, "Directional couplers," in *Advances in Microwaves*, vol. 1. New York: Academic Press, 1966, pp. 115–209.

Shunt-Connected Microstrip Radial Stubs

F. GIANNINI, SENIOR MEMBER, IEEE, M. RUGGIERI, AND J. VRBA

Abstract **— Radial-line stubs provide an interesting alternative to low-impedance conventional straight stubs. They are useful as filter elements in both series and shunt configurations. In this short paper, the planar circuit**

Manuscript received July 8, 1985; revised October 25, 1985.

F. Giannini and M. Ruggieri are with the Dipartimento di Ingegneria Elettronica, II Universita Degli Studi di Roma, Via Orazio Raimondo 00173, Roma, Italy.
J. Vrba is with the Department of Electromagnetic Field, Czech Technical University, 16627 Praha, Czechoslovakia.

IEEE Log Number 8406855.